

Ordering and Dynamics of Vibrated Hard Squares

Lee Walsh¹ and Narayanan Menon^{1,2}

¹Department of Physics, University of Massachusetts, Amherst, USA

²TIFR Centre for Interdisciplinary Science, Hyderabad, India

E-mail: lawalsh@physics.umass.edu, menon@physics.umass.edu

Abstract. We study an experimental system of hard granular squares in two dimensions, energized by vibration. The interplay of order in the orientations and positions of anisotropic particles allows for a rich set of phases. We measure the structure and dynamics of steady states as a function of particle density. This allows us to identify a progression of phases in which a low density isotropic fluid gives way to a phase with tetratic orientational order, short-range translational correlations, and slowed rotational dynamics. In this range of density we also observe a coupling between the molecular orientational order and bond-orientational order. At higher densities, the particles freeze into a translationally and orientationally ordered square crystalline phase in which translational diffusion is suppressed.

Keywords: granular matter, phase diagrams (experiments), jamming and packing, driven diffusive systems (experiments)

1. Introduction

An assembly of hard squares in two dimensions presents a variety of potential spatial orders. Hard particles form thermodynamic phases dictated solely by the entropy of their geometric packing; temperature is irrelevant as the interaction potential has no finite energy scale. Particles with asymmetric shapes have anisotropic constraints of self-avoidance and therefore pack in complex phases. Squares are an obvious point of entry into this complexity because they can tile the plane without frustration. However, there has been relatively little investigation into the phases formed by this simple shape as a function of density, and still less of the dynamics within these phases.

The phase diagram of isotropic hard disks [1–3] offers a context for the ordering of asymmetric particles. A two-dimensional crystal of disks has correlations in particle positions with algebraic (power-law) decay. As density is decreased the crystal melts into the hexatic phase in which the orientation of “bonds” between neighboring particles has algebraic correlations, which finally melts into an isotropic liquid phase. Anisotropic particles have both translational and rotational degrees of freedom, each of which may order independently or become coupled, providing the possibility of new classes of order. For example, particle (or “molecular”) orientations may order independently of their locations, giving rise to phases with global orientational order in the absence of translational order, e.g. the nematic liquid crystal phase. These phases in two

dimensions have been explored using various rigid shapes with a two-fold rotational symmetry, such as rectangles [4,5], ellipses [6], or rods [7–9]. Some of these two-fold symmetric particles yield phases with four-fold symmetry. This has also been demonstrated by density functional theories [10,11]. Minor differences in shape can have drastic effects on the phase diagram of such systems in two dimensions [12–14], and three dimensions [15–17].

Existing work on shapes with four-fold symmetry — such as squares — is limited, but raises interesting questions about the phase diagram. Monte Carlo simulations of an equilibrium hard-square system by Wojciechowski and Frenkel suggest a four-fold tetratic phase with longer-range orientational order than translational order [18]. By contrast, in experiments on a colloidal suspension of square-shaped tiles osmotically constrained to a surface, Zhao *et al.* found no evidence of an orientationally ordered state [19]. At densities above that of the isotropic phase, they instead observed a “hexagonal rotator” phase where particles form a plastic crystal with hexagonal bond-orientational order but no molecular-orientational order. At higher densities, the system enters a rhombic phase with a lattice angle that continuously approaches the 90° angle of a square crystal at full packing.

| Molec. | Bond | Transl. | Phase |
|--------|------|---------|--------------------------------------|
| — | — | — | isotropic liquid |
| X | — | — | 4-fold molecular orientational order |
| — | X | — | 4-fold bond-orientational order |
| X | X | — | tetratic |
| — | X | X | plastic (rotator) crystal |
| X | X | X | square crystal |

Table 1. Potential phases from combinations of translational, bond-, and molecular-orientational order. “—” indicates short-range order with exponentially decaying spatial correlations; “X” indicates quasi-long-range order with algebraic decay.

Monte Carlo simulations by Avendaño and Escobedo [12] indicate that particle shape is the critical difference between these two studies. They found that squares with sufficiently rounded corners form the hexagonal rotator phase observed by Zhao, *et al.* [19], whereas squares with sharper corners show indications of a tetratic-like phase before crystallization [18].

Our present study is motivated by the absence of experiments in the hard square limit. Furthermore, individual particle dynamics can be measured via experiment, which Monte Carlo simulations do not capture. In this work we present experimental observations of structure and translational and rotational dynamics of the steady states of a system of vibrated hard granular squares. The macroscopic nature of the system gives us the advantage of precise control over the particle properties, including shape [8,20–22]. This allows us to achieve the limit of sufficiently sharp corners to accurately represent hard squares [12]. Our system size is necessarily small, though comparable to previous simulations and experiments [9,12,18,19]. As a result, transitions are rounded off due to finite number, and long-range correlations are truncated by the boundary.

We find a progression from an isotropic disordered fluid at low density, through a fluid

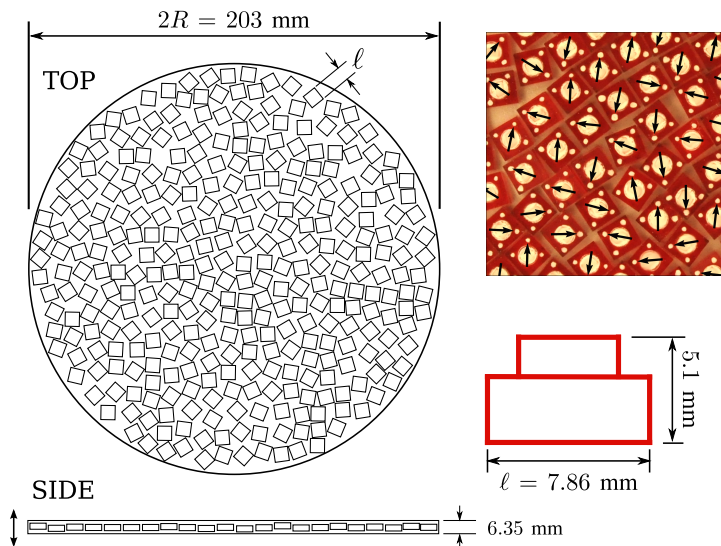


Figure 1. Experimental setup. Particles ($N \approx 500$) are constrained in a quasi-two-dimensional circular dish between an aluminum substrate and acrylic cover. The dish has diameter $2R = 203$ mm with height 6.35 mm, and particles have side length $\ell = 7.86 \pm 0.01$ mm and height 5.1 mm. Photo at upper right shows the particles (at density $\rho = 0.78$) painted with white tracking targets at center and three corners. Arrows show location and orientation of detected particles.

with orientational order, arriving at a solid with both orientational and translational order. The intermediate orientational order is tetratic, in which bond- and molecular-orientational order are coupled and each has four-fold symmetry. Neither hexagonal rotator nor rhombic phases are seen. The static structure analysis gives qualitative agreement with Monte Carlo simulations [12,18]. We also present new results on the dynamics of particles as a function of density. We find that rotational diffusion is suppressed relative to translational diffusion in the approach to the tetratic phase. At still higher densities, the transition to the solid is accompanied by the loss of translational diffusion.

2. Experiment

We confined square particles to a monolayer in a horizontal dish. Vertical vibration provides quasi-thermal noise in two dimensions and the particles diffuse in plane. The setup is shown in figure 1. Particles are hard plastic tiles (manufactured by LEGO) with sides of length $\ell = 7.86 \pm 0.01$ mm and base height of 3.2 mm, plus a 1.9 mm high cylindrical protrusion on the top, for a total height of 5.1 mm. Corners have radius of curvature $\sigma/2 = 0.15 \pm 0.01$ mm, giving a corner-rounding-to-length ratio $\zeta = \sigma/\ell = 0.04$ [12]. Their mass is 204 ± 1 mg. The particles are contained in a circular aluminum dish of diameter $2R = 20.3$ cm with an acrylic lid that maintains a vertical gap of 6.35 mm (1.25 particle height). The dish is coupled to a permanent magnet electrodynamic shaker (LDS V456 shaker and PA1000L amplifier), which vibrates the

dish vertically following sine-wave motion with peak acceleration $\Gamma \approx 10g$ at frequency $f = 50$ Hz.

Particles were imaged from above with a high-speed video camera (Vision Research Phantom v7.1) to measure displacements, and a DSLR camera (Nikon D5000) to measure positions. They are marked with dots for detection of position and orientation, as shown in figure 1. For dynamic measurements, we uniquely identified and tracked particles through 120-fps video. Positional uncertainty, primarily from lighting and imaging, is 0.25 pixels, which corresponds to 0.01ℓ in video images and 0.002ℓ in still images, where ℓ is the particle size. For all data, orientational uncertainty is 0.02 rad and is dominated by inaccuracy in marking dot location.

We controlled the density (packing fraction) ρ by varying the number of particles N in the dish. Particles tend to align with the dish walls, therefore a margin of two particle layers is excluded from the analysis and density calculations. The choice of the margin size affects the density by up to ± 0.004 , while the temporal fluctuations of the density are of order ± 0.005 .

In this nonequilibrium system, energy is fed to particles via collisions with the vibrating cell. Collisions between particles and the bottom plate, the lid, and other particles are inelastic, and kinetic energy is dissipated quickly. Likewise, momentum of the particles is not conserved due to collisions and friction with the substrate. The nonequilibrium drive from the vertical vibration provides noise that leads to motion in the horizontal direction. The symmetry of the resultant impulse on the particle matches the symmetry of the particle shape, but the long-term motion of the tiles is isotropic.

3. Structure

In this section, we study the emergence of ordered phases by capturing static images of the system over a range of densities. The images were taken at time intervals (minutes) long enough compared to typical diffusion times (seconds) to obtain statistically independent configurations of the particles. We characterized spatial order with order parameters and correlation functions computed from particle positions and orientations.

3.1. Positional Order

We first consider translational order by studying particle positions, regardless of their orientations. Translational order can be quantified by the radial distribution function $g(r)$, which gives the probability density of finding two particles separated by distance r . Our measurement is shown in figure 2. As density increases, we observe sharper and taller peaks; the peaks are asymmetric, with sharp lower bounds at integer values of r/ℓ , which correspond to particle separation in a perfect square packing. At high densities ($\rho \gtrsim 0.78$), a shoulder and then a new peak begins to form near $r/\ell = \sqrt{2}$ corresponding to the second-nearest neighbor distance in a square crystal.

The characteristic length of translational order can be determined from the functional form and length scale of the decay envelope of $g(r)$. Short-range order is associated with exponential decay $e^{-r/L}$, while quasi-long-range order is indicated by algebraic decay r^{-n} . We extract the peaks from $g(r)$, and plot them with fits to both exponential

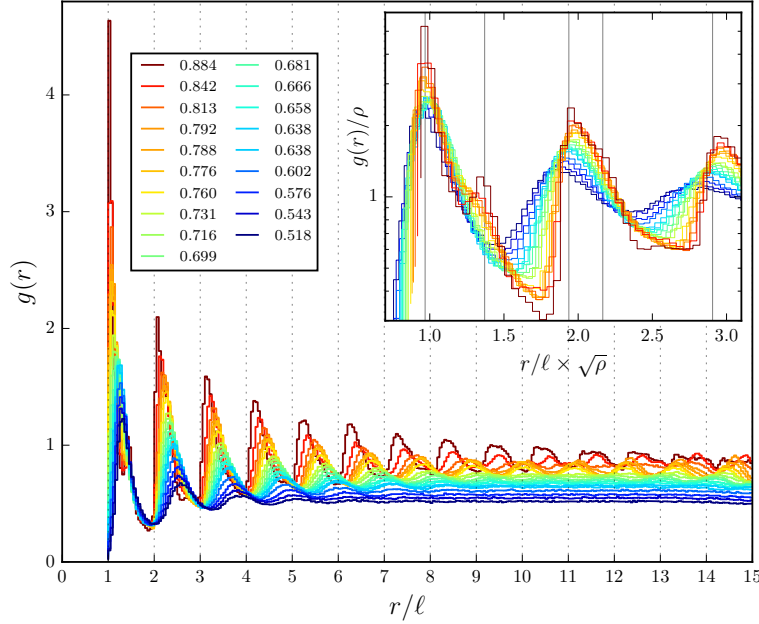


Figure 2. The radial distribution function $g(r)$ at various densities. The spatial range of translational order increases with density. Inset: Detail of the nearest peaks, rescaled by density to show the evolution of square structure as the density is increased. Vertical lines mark $1, \sqrt{2}, 2, \sqrt{5},$ and 3 times the average inter-peak spacing. The developing peaks and shoulders near $\sqrt{2}$ and $\sqrt{5}$ indicate the emergence of square-crystalline order around densities $\rho \gtrsim 0.78$.

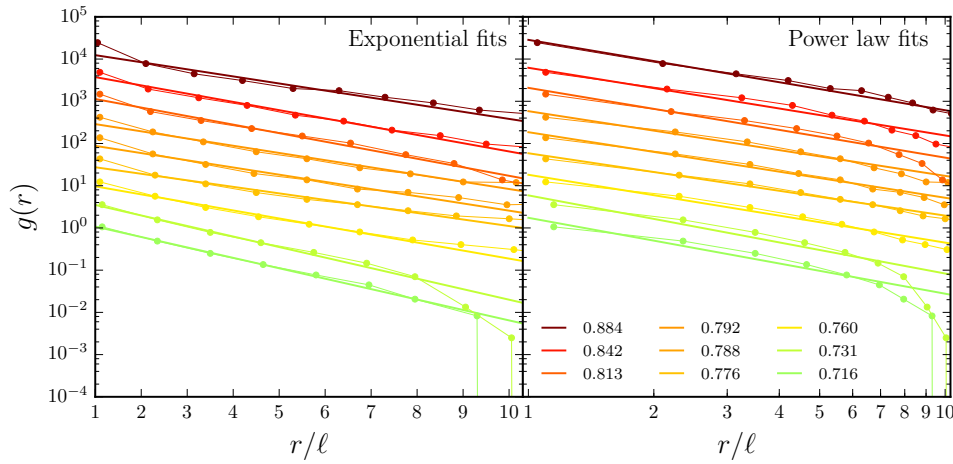


Figure 3. Fits to $g(r)$ peaks. The decay shape of the peak envelope for $g(r)$ shows the extent of translational order. Shown are the peaks from $g(r)$ with fits to exponential (left) and power-law (right) decay functions. Curves of different density are vertically offset by a factor of 3 for clarity; the lowest curve has no offset.

and algebraic decay functions in figure 3. At densities of 0.76 and higher, exponential decay clearly underestimates correlations at large r/ℓ . At the two lowest densities shown ($\rho = 0.72, 0.73$), the power law overestimates the correlations, which have a pronounced downward curvature over all r . It is difficult to unambiguously identify a transition density; however, from examination of quality of fits, our best estimate for the transition from short-range to quasi-long-range translational order is $\rho \approx 0.76$.

A subtler form of spatial ordering can be studied by measuring the angles of the “bonds” connecting the centers of pairs of neighboring particles. (The bond angle θ_{jk} does not depend on the orientation of individual particles, as illustrated in the inset diagram in figure 4, left). The global bond orientation order parameter measures m -fold lattice orientation symmetry, and is given by:

$$\Psi_m = \left| \langle e^{im\theta_{jk}} \rangle_{jk} \right|$$

where θ_{jk} is the bond angle of neighboring particles j and k . The average is calculated over all neighboring pairs; for $m = 4$, neighbors are the four nearest particles, and for $m = 6$, neighbors are given by the Delaunay triangulation. Ψ_m are shown in figure 4 (left). We find that Ψ_6 remains near zero for all densities, indicating the absence of hexagonal order; thus the hexagonal rotator phase [19] is not found for hard squares. On the other hand, Ψ_4 shows a marked increase in square symmetry as density increases.

The preceding observations of the translational degrees of freedom indicate the onset of translational order near $\rho \gtrsim 0.76$, which follows four-fold bond-orientational order at lower densities. In the next section, we report molecular orientational order, followed by a discussion of spatial correlations of both positional and orientational order.

3.2. Particle Orientational Order

The “molecular” orientation of the individual particles is given by the angle γ_i of the tile, illustrated in the inset diagram in figure 4 (right). Global orientational order of the system is given by the particle orientation order parameter:

$$\Phi_m = \left| \langle e^{im\gamma_i} \rangle_i \right|$$

where $m = 4$ is the rotational symmetry and the average is taken over all particles i .

We find that Φ_4 begins increasing above the noise at densities in the range 0.64 to 0.68 with a marked rise above $\rho \gtrsim 0.72$ (figure 4, right). This indicates an increase in global tetratic (four-fold orientational) order, analogous to nematic (two-fold) order.

A different, local measure of orientational alignment is the distribution of orientation differences between neighboring particles, as defined through a Delaunay triangulation. The width of this distribution is the normalized standard deviation of these angle differences:

$$\Delta_m = 1 - \frac{\sqrt{12}}{\pi/2} \sqrt{\langle (\delta\gamma_{ij})^2 \rangle_{\{i,j\}}}$$

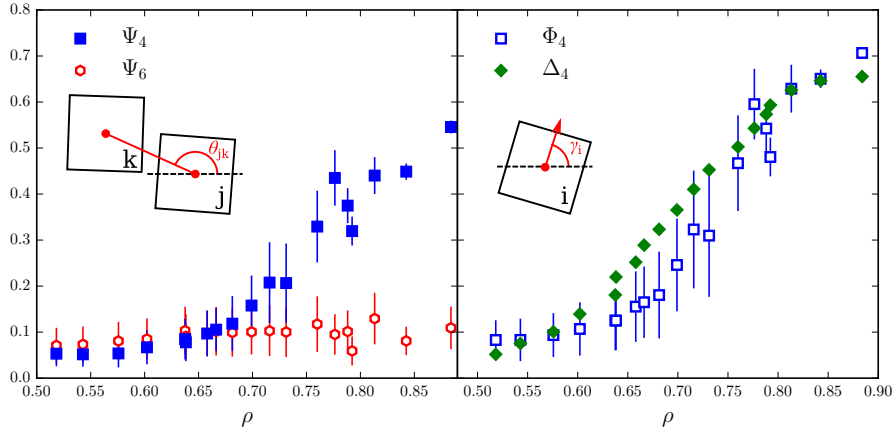


Figure 4. Order Parameters. Left: The bond orientation order parameter Ψ_m for both $m = 4$ and $m = 6$. Inset diagram shows the bond angle θ . We see a clear increase in four-fold bond angle order with none for six-fold order, indicating an approach toward square crystalline order with no evidence for the hexagonal rotator phase at any density. Right: The particle orientation order parameters Φ_4 and Δ_4 . Inset diagram shows the particle orientation angle γ . Both parameters show a parallel increase in four-fold particle orientation (tetratic) order, indicating a phase with stronger orientational order than translational order.

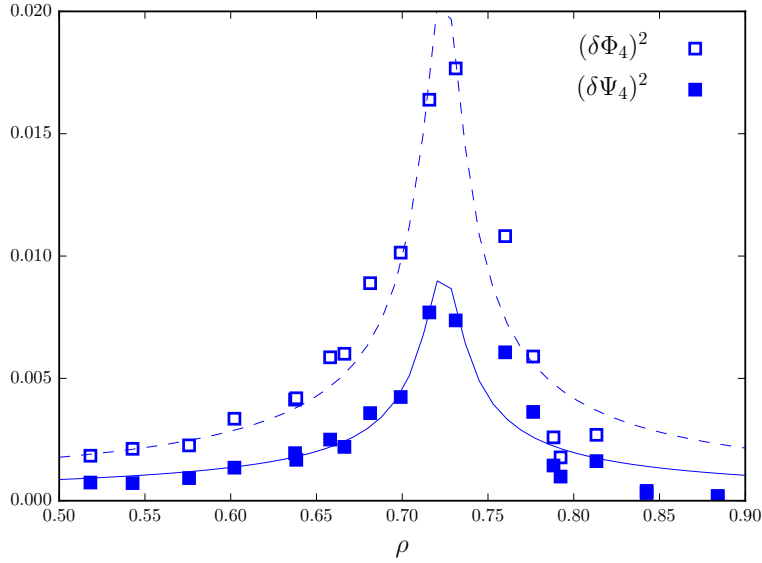


Figure 5. Order Parameter Variances. The variances over long times of the order parameters shown in figure 4. The peak in the variance indicates the existence of a phase transition. This occurs simultaneously at density $\rho_c = 0.72$ for both orientational and translational order, but the peak for orientational is stronger. The curves are best fits to $|\rho - \rho_c|^{-\eta}$, from which we extract the transition density. This indicates a coupling during this transition of these two degrees of freedom, dominated by orientational order.

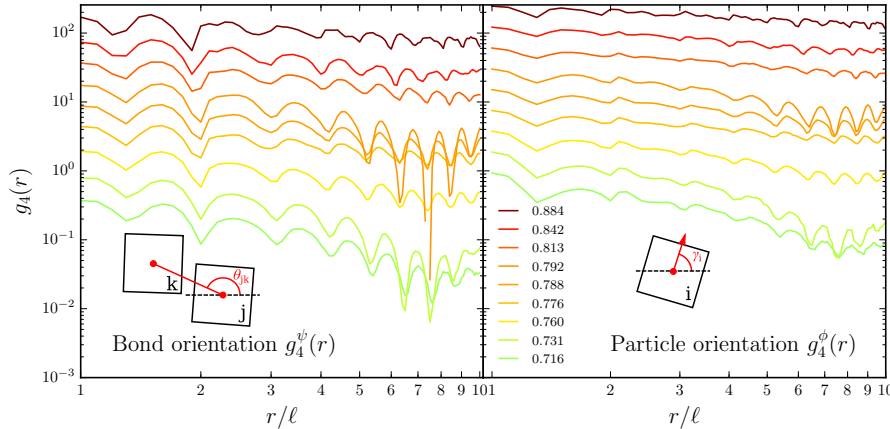


Figure 6. Correlation functions of the order parameters. The correlation functions for bond orientation $g_m^\psi(r)$ (left) and particle orientation $g_m^\phi(r)$ (right). Curves of different density are vertically offset by a factor of 2 for clarity; the lowest curve has no offset. We find that bond orientation correlation has a lower amplitude and decays more quickly than the particle orientation correlation.

where $\delta\gamma_{ij}$ is the smallest angle between the orientations (measured modulo $2\pi/m$) of neighboring particles i and j , and the average is over all such pairs. The values of Δ_4 agree with the global orientational parameter Φ_4 as shown in figure 4, reflecting the concurrent emergence of local and global orientational alignment.

Bond-orientation order Ψ_4 appears at nearly the same density as Φ_4 . To better pin down the transition densities, we consider the order parameter variances, which should diverge at the transition (figure 5). For both the particle- and bond-orientation, the ensemble variance in the order parameter peaks near density $\rho = 0.72$, indicating a coupling between the translational and orientational degrees of freedom. The smaller amplitude of the bond-orientational order parameter suggests that the transition may be driven by the ordering of particle orientations.

We measure the spatial extent of the above types of order by computing the associated correlation functions. The form of the decay of each correlation function allows us to distinguish between short-range order and quasi-long-range order; the former is characterized by exponential decay and the latter by algebraic decay.

The extent of particle orientational order is described by:

$$g_m^\phi(r) = \langle \cos m(\gamma_i - \gamma_j) \rangle_{r_{ij}=r}$$

where the average is taken over all pairs separated by distance r . Our data is shown in figure 6, left. We find that exponential fits underestimate the correlation for densities above $\rho \approx 0.73$.

We compare this to the correlation function for the bond orientational order parameter ψ_m , given by:

$$g_m^\psi(r) = \langle \psi_m^*(r_j) \psi_m(r_k) \rangle_{r_{ij}=r}$$

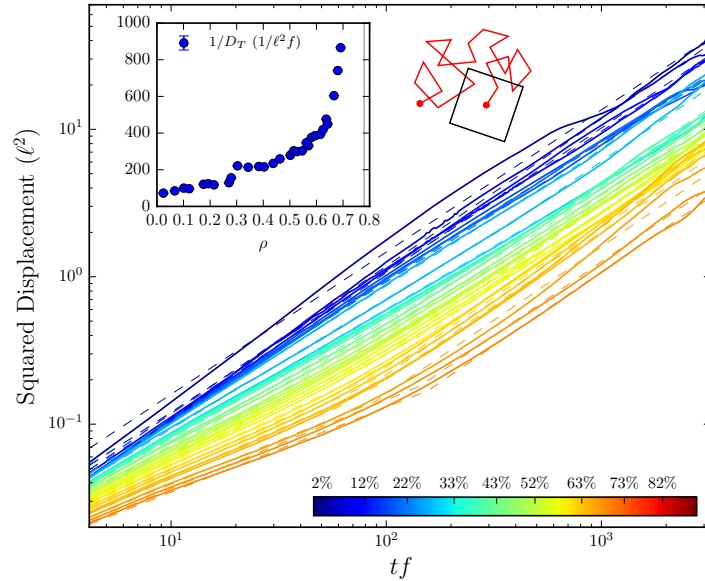


Figure 7. Mean Squared Displacement (in units of particle size ℓ) versus time (in units of vibration periods $1/f$). Particle motion at densities ranging from 0.03 to 0.70 shows diffusive behavior at low densities with a decreasing coefficient of diffusion. At densities above 0.30, motion is not diffusive at short times, becoming diffusive only after approximately $tf \approx 10^2$ vibration periods. Inverse Coefficient of Diffusion (inset): Fits for coefficient of diffusion D_T are made to data for $tf > 500$.

Here $\psi_m(r_i)$ is the bond-orientational order parameter calculated for the neighbors of particle i . The average is taken over all pairs separated by distance r . The form of this correlation (figure 6, right) matches that of $g^\phi(r)$, but has lower amplitude, consistent with the respective order parameters. We observe significantly smaller oscillations in $g^\phi(r)$ compared with $g^\psi(r)$. This indicates that bond-orientational order is weak at positions incompatible with square-crystalline order, i.e., at valleys in $g(r)$, while molecular orientational order is less sensitive to position.

4. Dynamics

The rotational and translational dynamics of particles reflect the constraints imposed by the spatial order in a phase. We track the locations $\vec{x}(t)$ and orientations $\theta(t)$ of particles as a function of time, from which we compute the mean squared displacement:

$$\Delta \vec{x}^2(t) = \left\langle [\vec{x}_i(t_0 + t) - \vec{x}_i(t_0)]^2 \right\rangle_{t_0, i}$$

where the average is taken over initial times t_0 and all particles i . The mean squared angular displacement is defined similarly:

$$\Delta \theta^2(t) = \left\langle [\theta_i(t_0 + t) - \theta_i(t_0)]^2 \right\rangle_{t_0, i}$$

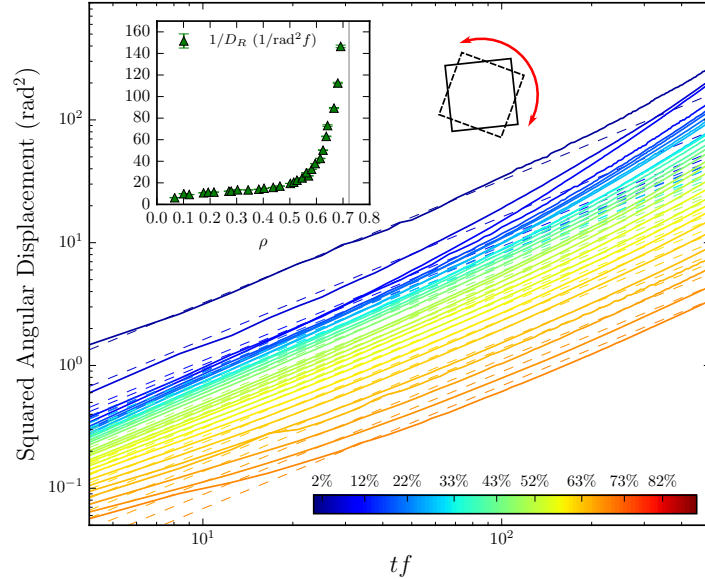


Figure 8. Mean Squared Angular Displacement, with time shown in units of vibration periods $1/f$. Particle motion at densities ranging from 0.03 to 0.70 shows diffusive behavior at low densities with a decreasing coefficient of diffusion. The mean squared angular displacement is diffusive at short times, but at long times rotational motion is super-diffusive. Inverse Coefficient of Angular Diffusion (inset): Fits for coefficient of angular diffusion D_R are made to data for $tf < 100$.

From each mean squared displacement, translational and rotational, we obtain the coefficients of diffusion D_T and D_R by fitting a power law of the form Dt to the data within the diffusive regime (figures 7 and 8). As density is increased, diffusion is slowed by collisions with neighboring particles. Both coefficients decrease with increasing density, as shown in the plots of $1/D$ in the insets of figures 7 and 8. At higher densities, particles become caged for short times and show a sub-diffusive regime before the long-time behavior becomes diffusive.† As the density approaches a critical value, the behavior of the diffusion coefficients is consistent with a power law, shown plotted against $\rho - \rho_c$ in figure 9, left.

To investigate the difference between translational and orientational order, we compare D_T and D_R . The rotational diffusion slows as it approaches $\rho_c^R = 0.72$, which is the same density at which the orientational order parameter variance peaks (figure 5). The translational diffusion freezes at $\rho_c^T = 0.78$, coinciding with the emergence of square crystalline signatures in $g(r)$ (figure 2). Their relative evolution can be seen directly without fitting by considering the decreasing ratio D_R/D_T above $\rho \approx 0.55$, shown in figure 9, right. Thus the onset of order constrains rotation at lower densities than it constrains translation.

† At very long times, we observe super-diffusive behavior, which results from a weak preference for one direction or the other in some particles. Rotation is unbiased when averaged over all particles.

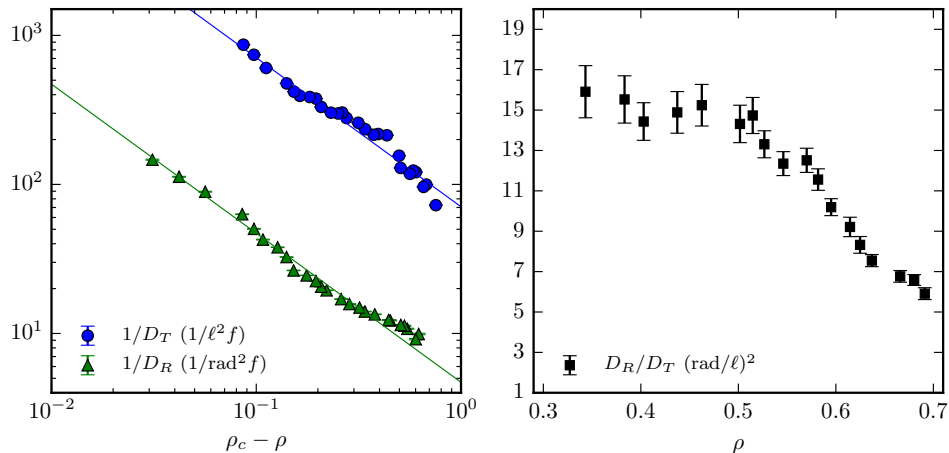


Figure 9. Coefficients of Translational and Rotational Diffusion. Left: The coefficients plotted on a log-log scale versus $\rho_c - \rho$, showing power-law divergence. The values $\rho_c^R = 0.72$ and $\rho_c^T = 0.78$ are determined by best fit to $|\rho - \rho_c|^{-1}$. Right: the ratio of rotational to translational diffusion D_R/D_T falls from its dilute limit as the density is increased, indicating a relative freezing of rotation compared with translation.

5. Conclusion

In our system of vibrated hard squares, increasing density gives rise to an increasing degree of order in the particle positions and orientations. At low density, packings are positionally and orientationally isotropic. Increasing density first leads to tetratic orientational order in the range $0.72 \lesssim \rho \lesssim 0.77$. This phase is characterized by quasi-long-range, four-fold order in particle orientation with short-range translational order. With further increases in density, beyond $\rho \approx 0.77$, the system tends toward a quasi-long-range translationally ordered square phase. No evidence is found for hexagonal positional order at any density.

| Molec. | Bond | Transl. | Phase | Density range |
|--------|------|---------|---------------------------|---------------|
| — | — | — | isotropic liquid | 0.00–0.72 |
| X | — | — | molecular orient | — |
| — | X | — | bond-orient | — |
| X | X | — | tetratic | 0.72–0.77 |
| — | X | X | plastic (rotator) crystal | — |
| X | X | X | square crystal | 0.77–1.00 |

Table 2. Densities of observed phases. Phase boundary between tetratic and square crystal estimated at $\rho = 0.76$ and 0.78 by $g(r)$ decay and by translational diffusion D_T .

Bond-orientational order, determined by particle positions alone, increases in the same density range where molecular-orientational order sets in, though with smaller amplitude and shorter-ranged correlations. Though these are distinct kinds of order in

independent degrees of freedom, their coexistence is not surprising because position and orientation are not separable in the pair interaction [23,24].

To our knowledge, this is the first experimental study of the hard-square limit. This granular system displays a sequence of phases consistent with equilibrium Monte Carlo simulations reported in [12] and [18]. As in those studies, the limited system size restricts structural analysis and smooths out transitions, making it difficult to pinpoint transition densities or study critical behaviour. However, measurements of the dynamics of the system — inaccessible by Monte Carlo — strengthen the evidence for the sequence of phases. In particular, the ratio of translational and rotational diffusion constants serves as a useful tool to show that orientational freezing precedes translational freezing.

5.1. Acknowledgements

We wish to thank JL Machta and JD Paulsen for helpful suggestions and conversations. This work was supported by NSF-DMR 1207778 and 1506750.

5.2. References

- [1] Kosterlitz J M and Thouless D J, 1973 *J. Phys. C: Solid State Phys.* **6** 1181
- [2] Nelson D and Halperin B, 1979 *Phys. Rev. B* **19** 2457–84
- [3] Young A, 1979 *Phys. Rev. B* **19** 1855–66
- [4] Donev A, Burton J, Stillinger F and Torquato S, 2006 *Phys. Rev. B* **73** 054109
- [5] Zhao K, Harrison C, Huse D, Russel W B and Chaikin P M, 2007 *Phys. Rev. E* **76** 040401
- [6] Cuesta J A and Frenkel D, 1990 *Phys. Rev. A* **42** 2126–36
- [7] Bates M and Frenkel D, 2000 *J. Chem. Phys.* **112** 10034–41
- [8] Narayan V, Menon N and Ramaswamy S, 2006 *J Stat Mech* **2006** P01005
- [9] Müller T, de las Heras D, Rehberg I and Huang K, 2015 *Phys. Rev. E* **91** 062207
- [10] Geng J and Selinger J V, 2009 *Phys. Rev. E* **80** 011707
- [11] Martínez-Ratón Y and Velasco E, 2009 *Phys. Rev. E* **79** 011711
- [12] Avendaño C and Escobedo F A, 2012 *Soft Matter* **8** 4675–81
- [13] Martínez-Ratón Y, Velasco E and Mederos L, 2005 *J. Chem. Phys.* **122**
- [14] Jiao Y, Stillinger F H and Torquato S, 2008 *Phys. Rev. Lett.* **100** 245504
- [15] Rossi L, Soni V, Ashton D J, Pine D J, Philipse A P, Chaikin P M, Dijkstra M, Sacanna S and Irvine W T M, 2015 *PNAS* **112** 5286–90
- [16] Batten R D, Stillinger F H and Torquato S, 2010 *Phys. Rev. E* **81** 061105
- [17] Damasceno P F, Engel M and Glotzer S C, 2012 *ACS Nano* **6** 609–14
- [18] Wojciechowski K W and Frenkel D, 2004 *Comput. Methods* **10** 235–55
- [19] Zhao K, Bruinsma R and Mason T G, 2011 *PNAS* **108** 2684–7
- [20] Reis P, Ingale R and Shattuck M, 2006 *Phys. Rev. Lett.* **96** 258001
- [21] Galanis J, Harries D, Sackett D, Losert W and Nossal R, 2006 *Phys. Rev. Lett.* **96** 028002
- [22] Safford K, Kantor Y, Kardar M and Kudrolli A, 2009 *Phys. Rev. E* **79** 061304
- [23] Nelson D and Halperin B, 1980 *Phys. Rev. B* **21** 5312–29
- [24] Gingras M, Holdsworth P and Bergersen B, 1990 *Phys. Rev. A* **41** 6786